Reduction of irregular view-sampling artifacts in a stationary gantry CT scanner

Alexander Katsevich[a,b,*], **Seongjin Yoon**[a], **Michael Frenkel**[a], **Ed Morton**[c], **William Thompson**[c]

[a]iTomography Corp., Texas Medical Center Innovation Institute, 2450 Holcombe Blvd, Houston, TX 77021, USA
[b]University of Central Florida, Mathematics Department, Orlando, FL 32816, USA
[c]Rapiscan Systems, 2805 Columbia St, Torrance, CA 90503, USA

Abstract. We propose an FBP reconstruction algorithm for a stationary gantry CT scanner with distributed sources. The sources are fired in quasi-random order to improve data completeness across the field of view (FOV). The downsides of that are two-fold. The neighboring sources are fired non-sequentially, so the view derivative should be avoided. Second, the angular distribution of rays through each voxel is non-uniform and varies across the FOV. To overcome these challenges we incorporate a weight function into an FDK-type reconstruction algorithm, and integrate by parts to avoid view differentiation. Results of experiments with simulated data confirm that a properly selected weight significantly reduces irregular view sampling streaks.

Keywords: image reconstruction, weight function, non-uniform view sampling, artifact reduction.

*Alexander Katsevich, alexander@itomography.com

1 Introduction

Most of CT scanners in operation today collect data in a conventional way. The detector is either flat or curved (with pixels distributed on a uniform grid), and the source moves along a well-defined trajectory (e.g., circular or helical) in a sequential way. For such scanners, efficient and high quality image reconstruction is well established. Reconstruction algorithms range from analytic (i.e., formula-based) to iterative. Stationary gantry CT (SGCT) with a distributed source and stationary detector in the context of security scanning poses unique challenges for image reconstruction. As is shown in Ref. 1, to achieve uniform illumination of the inspection tunnel, the order in which the X-ray sources are fired should be sufficiently random. Hence, the notion of source trajectory loses much of its meaning. The sources that are located close to each other in space are fired nonsequentially at random times. This creates two complications. (1) Since the object moves sufficiently far during the time when any two neighboring sources are fired, one should avoid calculation of the derivative along the view direction. (2) The illumination pattern of any voxel is highly anisotropic and varies significantly across the field of view. In this case, direct application of conventional formula-based reconstruction will lead to significant irregular view sampling artifacts. Finally, because of time constraints for performing near real-time SGCT imaging, the reconstruction algorithm has to be of the filtered-backprojection (FBP) type.

In this paper we propose an FBP reconstruction algorithm that overcomes the above challenges. Initially, we propose a 2D version of the algorithm, and then extend it to 3D in the FDK-type fashion. Nevertheless, the 3D nature of the reconstruction problem is reflected in an essential way since the time each voxel remains visible on the detector determines the illumination patterns of the voxel. These illumination patterns are then used in the algorithm. The algorithm does not use view differentiation, so it is of the No View-Differentiation (NVD) type. Note that the proposed

15th International Meeting on Fully Three-Dimensional Image Reconstruction in Radiology and Nuclear Medicine, edited by Scott D. Metzler, Samuel Matej, Proc. of SPIE Vol. 11072, 110720G · © 2019 SPIE · CCC code: 0277-786X/19/$18 · doi: 10.1117/12.2534878

algorithm applies to a wide range of source trajectories, including, e.g., rectangular (considered in this paper), circular, elliptical, etc.

2 Description of the algorithm

2.1 Mathematical formulation of the algorithm

We start in the 2D setting. Let $f(\vec{x})$, $\vec{x} = (x_1, x_2)$, denote the object to be reconstructed, and $\hat{f}(\vec{y}, \theta)$ denote its Radon (fan-beam) transform. Here $\vec{y}$ is the source position, and $\Theta = (\cos\theta, \sin\theta)$ is the fan angle. Our algorithm is based on the formula (26) in Ref. 2 (which, in turn, is based on the ideas in Ref. 3). The formula reads:

$$f(\vec{x}) = -\frac{1}{4\pi}\int_S \frac{w(\vec{x},\theta)}{|\vec{x}-\vec{y}(s)|}\int_0^{2\pi}\frac{\partial_s \hat{f}(\vec{y}(s),\gamma)}{\sin(\gamma-\theta)}d\gamma\, ds,\ (\cos\theta,\sin\theta) = \frac{\vec{x}-\vec{y}(s)}{|\vec{x}-\vec{y}(s)|}. \tag{1}$$

Here S is the parametric interval that describes the source trajectory $\vec{y}(s)$, and $w(\vec{x},\theta)$ is the weight that controls the utilization of redundant information. The latter can be almost any function that satisfies the normalization condition $w(\vec{x},\theta)+w(\vec{x},\theta+\pi) = 1$ for all $\vec{x}$ and $\theta \in [0, 2\pi)$. Integrating by parts in (1) with respect to s similarly to Ref. 4, we remove the view-derivative. The resulting formula for the cylindrical detector is

$$\begin{aligned} f(\vec{x}) = {} & \frac{1}{2\pi}\int_S \left(\frac{\partial}{\partial s}\frac{w(\vec{x},s)}{|\vec{x}-\vec{y}(s)|}\right)\int_0^{2\pi}\frac{\hat{f}(\vec{y}(s),\gamma)}{\sin(\gamma-\theta(\vec{x},s))}d\gamma\, ds \\ & + \frac{1}{2\pi}\int_S \frac{w(\vec{x},s)|\vec{y}'(s)\times(\vec{x}-\vec{y}(s))|}{|\vec{x}-\vec{y}(s)|^3}\int_0^{2\pi}\frac{\partial_\gamma \hat{f}(\vec{y}(s),\gamma)}{\sin(\gamma-\theta(\vec{x},s))}d\gamma\, ds. \end{aligned} \tag{2}$$

An analogous formula for a flat detector is as follows:

$$\begin{aligned} f(\vec{x}) = {} & \frac{1}{2\pi}\int_S \left(\frac{w(\vec{x},s)\big(\vec{y}'(s)\cdot(\vec{x}-\vec{y}(s))\big)}{|\vec{x}-\vec{y}(s)|^3} + \frac{w(\vec{x},s)'}{|\vec{x}-\vec{y}(s)|}\right) \\ & \cdot\sqrt{R^2+u_0^2(\vec{x},s)}\int_{-\infty}^{\infty}\frac{\hat{f}(\vec{y}(s),\gamma(u))/\sqrt{R^2+u^2}}{u-u_0(\vec{x},s)}du\, ds \\ & + \frac{1}{2\pi}\int_S \frac{w(\vec{x},s)|\vec{y}'(s)\times(\vec{x}-\vec{y}(s))|}{|\vec{x}-\vec{y}(s)|^3} \\ & \cdot\frac{\sqrt{R^2+u_0^2(\vec{x},s)}}{R}\int_{-\infty}^{\infty}\frac{\partial_u \hat{f}(\vec{y}(s),\gamma(u))\sqrt{R^2+u^2}}{u-u_0(\vec{x},s)}du\, ds. \end{aligned} \tag{3}$$

Consider the role of w in more detail. Mathematically, $w(\vec{x},\theta)$ is the weight with which the filtered data at the source $\vec{y}(s)$ contributes to the image at $\vec{x}$. Here $\vec{y}(s)$ is such that it satisfies the last equation in (1). Pick any $\vec{x}$ and $\theta \in [0, 2\pi)$, and find the pair of sources $\vec{y}(s_1)$, $\vec{y}(s_2)$ such that $\vec{x}$ is on the chord $[\vec{y}(s_1), \vec{y}(s_2)]$, and $(\cos\theta, \sin\theta) = (\vec{y}(s_2)-\vec{y}(s_1))/|\vec{y}(s_2)-\vec{y}(s_1)|$. The data at $\vec{y}(s_1)$ and $\vec{y}(s_2)$ contribute the same information to the image at $\vec{x}$ (in the context of helical CT, the points $\vec{y}(s_1)$ and $\vec{y}(s_2)$ are called π-partners, see Ref. 5). Hence, the freedom in the choice of w gives us

one possible way to accomodate the peculiarities of the scanner and improve image quality. For example, it may turn out that view sampling in a neighborhood of $\vec{y}(s_1)$ is finer than view sampling in a neighborhood of $\vec{y}(s_2)$. Therefore, we can increase $w(\vec{x},\theta)$ (the weight of the contribution of $\vec{y}(s_1)$), and decrease $w(\vec{x},\theta+\pi)$ (the weight of the contribution of $\vec{y}(s_2)$). Alternative approaches to optimize the weight are possible. An example of selecting w for the purpose of eliminating the backprojection weight is in Ref. 6. Earlier examples of using backprojection weights for cone beam CT are in Refs. 5,7.

As is shown in Ref. 8, more sophisticated methods for computing the view derivative (Refs. 8,9) provide resolution essentially similar to that of the NVD algorithms. However, in the SGCT case, the reconstruction algorithm is applied to cone beam data, in which neighboring sources collect views at fairly different locations along the axial (x_3) direction. Hence, differentiation between views may lead to artifacts that would not be present if all the views were along a smooth curve. In a similar fashion, even though integration by parts leads to a mathematically equivalent expression, the result may be a numerically non-equivalent formula due to cone beam approximations.

2.2 Illumination pattern and the choice of the weight function

As mentioned earlier, we select w that reduces streaks due to irregular view sampling. To do so, we compute a visibility map for every image plane. Let p denote the 2D index of an image pixel in the plane, and j denote the source index. The visibility map $m_s(p,j)$ contains binary information for each pixel-source pair (p,j). The map shows whether the image pixel p is visible (i.e., projects on the detector) from the source j, i.e. $m_s(p,j)=1$ if the p-th image pixel is visible from the j-th source, and $m_s(p,j)=0$ otherwise. Using the visibility map $m_s(p,j)$, a periodic Gaussian mixture density function in the angular domain $\rho(p,\theta)$ is first computed for each image pixel p. The Gaussian mixture approach uses the visibility map and gives a smooth function on the unit circle parametrized by θ:

$$\rho(p,\theta)=\sum_j m_s(p,j)\exp\left(-\frac{\min\left(|\theta-\theta_{(p,j)}|\,,\,2\pi-|\theta-\theta_{(p,j)}|\right)}{2\sigma_s^2}\right), \tag{4}$$

where $\theta_{(p,j)}=\theta(\vec{x}_p,s_j)$. To make sure w satisfies the normalization condition, we use the formula:

$$w_{(p,j)}=\frac{\rho(p,\theta_{(p,j)})^{t_w}}{\rho(p,\theta_{(p,j)})^{t_w}+\rho(p,\theta_{(p,j)}+\pi)^{t_w}},\ t_w\geq 0, \tag{5}$$

where t_w adjusts the weight bias between pi-partners. If t_w = 0, then $w=1/2$ for both pi-partners in each pair. If $t_w=\infty$, then the partner with the higher density between pi-partners will have weight $w=1$, and the other partner - weight $w=0$. Lower σ_s and higher t_w will decrease streak artifacts, but will also increase the numerical error since w becomes less smooth. Computing w for each slice $x_3=$ const is time consuming, and saving the pre-computed values takes large amount of memory. Fortunately, with large enough σ_s, the Gaussian mixture density for each slice is almost constant along x_3. So we use a single pre-computed w, which is averaged over several slices.

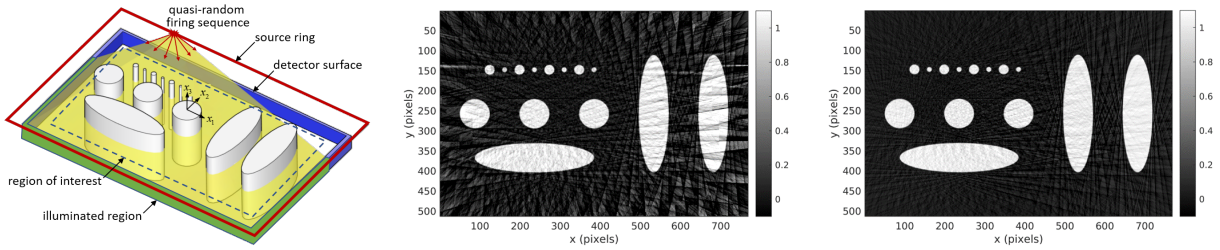

(a) (b) (c)

Fig 1 Numerical simulation results. (a) conceptual drawing of the SGCT scanner and the phantom objects, (b) reconstructed image with uniform weighting, (c) reconstructed image with visibility optimized weighting.

3 Numerical Experiments

The SGCT scanner consists of a ring of distributed sources along a rectangle, and a set of stationary detector modules arranged in a smaller rectangular surface surrounding the imaging region (see Fig. 1(a)). The detector is slightly offset along x_3 relative to the source ring to avoid beam interference. The sources are simulated to be mono-energetic and fired in a periodic quasi-random sequence. To test the performance of the proposed algorithm, we compare FDK-type NVD reconstruction with uniform weight $w = 0.5$ and with visibility optimized weight (5). We simulate noise-free data for a x_3-independent phantom consisting of water cylinders (see Fig. 1(a)). This experiment is designed to highlight the effects of the weight, which could otherwise be obscured by cone beam artifacts and noise. Even though the object is x_3-independent, the illumination pattern, visibility maps, and transmission data are all computed using the actual 3D geometry. Additional reconstructions with 3D phantoms and noisy data will be shown at the conference.

Figs. 1(b) and 1(c) show reconstruction results with uniform and visibility optimized weights, respectively. The intensity of the sparse-view streaks is significantly reduced by using an optimized weight. The improved image quality is especially important for automated image analysis, including threat detection.

References

1 W. M. Thompson, W. R. B. Lionheart, and D. Oberg, "Reduction of periodic artefacts for a switched-source x-ray CT machine by optimising the source firing pattern," in *Proceedings of the 12th Fully 3D Meeting. Lake Tahoe, California. June 16 - 21, 2013*, 345–348 (2013).

2 F. Noo, M. Defrise, R. Clackdoyle, *et al.*, "Image reconstruction from fan-beam projections on less than a short scan," *Physics in Medicine and Biology* **47**, 2525–2546 (2002).

3 A. Katsevich, "Theoretically exact filtered backprojection-type inversion algorithm for Spiral CT," *SIAM Journal on Applied Mathematics* **62**, 2012–2026 (2002).

4 A. Katsevich, K. Taguchi, and A. Zamyatin, "Formulation of four Katsevich algorithms in native geometry," *IEEE Transactions on Medical Imaging* **25**, 855–868 (2006).

5 T. Köhler, C. Bontus, and P. Koken, "The Radon-split method for helical cone-beam CT and its application to nongated reconstruction," *IEEE Transactions on Medical Imaging* **25**, 882–897 (2006).

6 F. Dennerlein, F. Noo, J. Hornegger, *et al.*, "Fan-beam filtered-backprojection reconstruction without backprojection weight," *Physics in Medicine and Biology* **52**, 3227–3240 (2007).

7 A. Katsevich, A. A. Zamyatin, and M. D. Silver, "Optimized Reconstruction Algorithm for Helical CT With Fractional Pitch Between 1PI and 3PI," *IEEE Transactions on Medical Imaging* **28**, 982–990 (2009).
8 F. Noo, S. Hoppe, F. Dennerlein, *et al.*, "A new scheme for view-dependent data differentiation in fan-beam and cone-beam computed tomography," *Physics in Medicine and Biology* **52**, 5393–5414 (2007).
9 A. Katsevich, "A note on computing the derivative at a constant direction," *Physics in Medicine and Biology* **56**, N53–N61 (2011).